SSC20-WKVI-02

Design and Prototyping of a Nanosatellite Laser Communications Terminal for the Cubesat Laser Infrared CrosslinK (CLICK) B/C Mission

Peter Grenfell, Paul Serra, Ondrej Cierny, William Kammerer, Grant Gunnison, Joseph Kusters, Cadence Payne, Kerri Cahoy
Dept. of Aeronautics and Astronautics, Massachusetts Institute of Technology, Cambridge, MA, USA
pgrenfel@mit.edu

Myles Clark, Tyler Ritz, Danielle Coogan, John Conklin
Dept. of Mechanical and Aerospace Engineering, University of Florida, Gainesville, FL, USA

David Mayer, Jan Stupl
NASA Ames Research Center, Moffett Field, CA, USA
77 Massachusetts Ave, Cambridge, MA, 02139

John Hanson
CrossTrac Engineering, Mountain View, CA, USA

Abstract

The CubeSat Laser Infrared CrossLink (CLICK) mission goal is to demonstrate a low cost, high data rate optical transceiver terminal with fine pointing and precision time transfer in a leq1.5U form factor. There are two phases to the technology demonstration for the CLICK mission: CLICK-A downlink, and then CLICK-B/C crosslink and downlink. The topic of this paper is the design and prototyping of the laser communications (lasercom) terminal for the CLICK-B/C phase. CLICK B/C consists of two identical 3U CubeSats from Blue Canyon Technologies that will be launched together in Low Earth Orbit to demonstrate crosslinks at ranges between 25 km and 580 km with a data rate of $\geq$20 Mbps and a ranging capability better than 0.5 m. Downlinks with data rates of $\geq$10 Mbps will also be demonstrated to the Portable Telescope for Lasercom (PorTeL) ground station. Link analysis using current parameters & experimental results predicts successful crosslink & downlink communications and ranging. Moreover, closed-loop 3σ fine pointing error is predicted to be less than 39.66μrad of the 121.0μrad $1/e^2$ transmit laser divergence. The status of the payload EDU and recent developments of the optomechanical and thermal designs are discussed.

1 Link Analysis and Experiment Operations

In this section, the CLICK B/C concept of operations (ConOps) will first be presented. Operations, link, and pointing analysis will be presented for crosslink experiments followed by downlink experiments. Figure 1 shows the CLICK B/C ConOps. The two spacecraft (CLICK B & CLICK C) will be co-deployed into low Earth orbit (LEO) in a string-of-pearls configuration: nearly equal orbital elements except for mean anomaly, which determines the relative range. The spacecraft are not equipped with propulsion, so differential drag manuevers will be used to establish the desired relative ranges by phasing the spacecraft such that their relative range gradually increases and then decreases over time during the mission. All spacecraft (S/C) operations, including differential drag and laser communications experiments, will be scheduled by the mission operations center (MOC) located at MIT via daily S-band radio contacts with three ground antennas in the KSAT Lite global network. The nominal minimum and maximum range requirements for crosslink demonstration experiments are 25 km and 580 km. Downlink experiments will also be conducted using an optical ground station (OGS) called the Portable Telescope for Lasercom (PorTeL) located at MIT Wallace Astrophysical Observatory. The CLICK B/C mission is the second phase of the CLICK mission. The first phase, CLICK A, will only demonstrate downlink experiments and will use the same OGS.[1]

At the scheduled time of initiation of the crosslink experiment (t_0), the two spacecraft use ephemeris information about each other provided by the MOC ground command to coarsely point at each

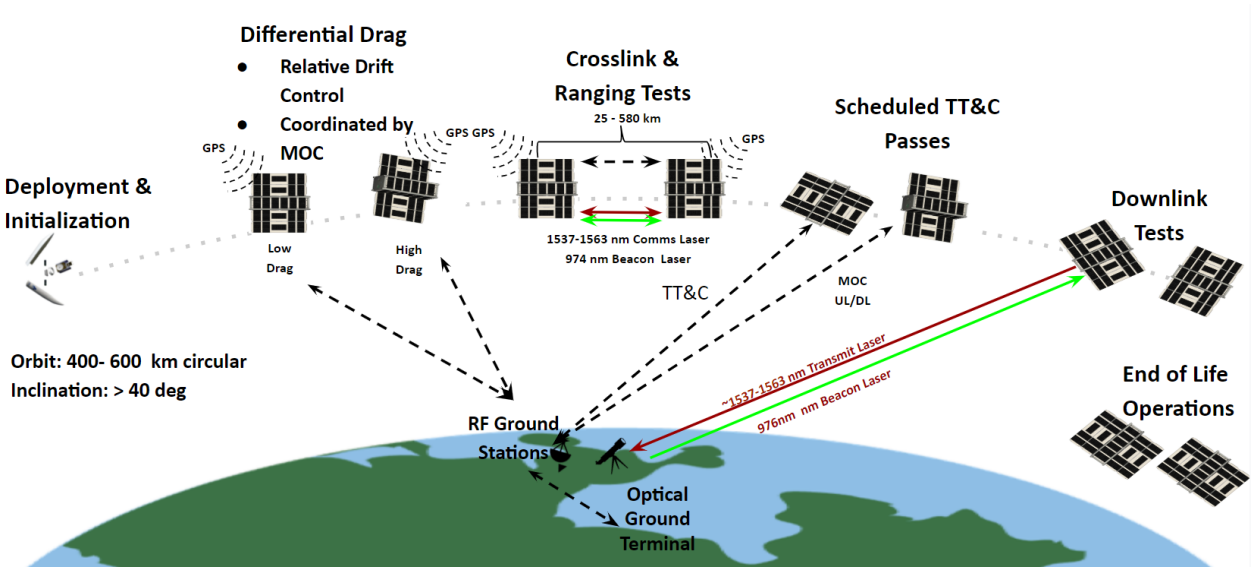

Figure 1: Concept of operations for the CLICK-B/C mission.

other in order to close an S-band radio crosslink. The radio crosslink is used to exchange navigation data generated in real time via the on-board Global Positioning System (GPS) receivers. This data is used to maintain accurate open-loop pointing of the payload apertures for up to 2 minutes prior to time-out if closed-loop tracking is not initiated. This pointing, acquisition, and tracking (PAT) phase is called coarse stage tracking in open-loop (CSTOL). During this time, a 974 nm, 3 kHz sine modulated, 250 mW average power beacon laser is activated by each payload, which is in-turn detected by each payload's wide field of view (FOV, 10.6°) tracking camera. The centroid data from the tracking camera is used to generate pointing angle errors for closed-loop spacecraft pointing, which is maintained for the remainder of the experiment. This phase is called coarse stage tracking in closed-loop (CSTCL). The beacon is then acquired by a narrow FOV (0.32°) quadrant photodiode detector (quadcell), which is used for closed-loop fine stage tracking (FST) of the transmit laser (1537 nm (B) or 1563 nm (C)) using a Mirrorcle fine/fast steering mirror (FSM). The beacon's sine modulation is used by the quadcell for filtering. This also aligns the received transmit signal onto the 0.24° FOV communications receiver: an avalanche photodiode detector (APD). The signal received by the APD will be processed in real-time on-board to achieve either a $\geq$ 20 Mbps communications link or ranging via time-transfer capability better than 0.5 m. The baseline link duration requirement is 5 minutes; however, the system is designed to be able to achieve a beacon link duration of up to 15 minutes and a communications link duration of up to 14 minutes.

Downlink experiments will be performed following a concept of operations similar to the CLICK A mission[1] with some variations described here. Once again, the spacecraft will point the payload apertures at the optical ground station's (OGS) geodetic coordinates starting 15 minutes prior to t_0, which is defined as the time at which the elevation angle of the spacecraft with respect to the OGS is zero degrees. The ground station's 975 nm, 2.5 W average power beacon will be pointed at the spacecraft using ephemeris data generated by orbit determination computations carried out by the MOC using the spacecraft's GPS telemetry data (this is the OGS's CSTOL phase). Note that the OGS beacon is now modulated at 3 kHz; hence, the average 2.5 W power rather than the 5 W power of the unmodulated CLICK A uplink beacon. The spacecraft pointing is sufficiently accurate such that the uplink beacon will be directly detected by the quadcell without needing the camera, although the capability for camera feedback to the spacecraft during downlink exists if needed. Once the beacon signal is detected by the quadcell, fine stage tracking (FST) initiates similar to that of the crosslink, except that the downlink is simplex as the OGS is receive-only. Upon activation of FST, the transmit laser is received by the OGS tracking camera, which enables the OGS's CSTCL phase for the remainder of the overpass. Simultaneously, the OGS's FST phase is

activated using its own FSM, which centers the received signal onto its APD for communications data rates that are required to be $\geq$ 10 Mbps. Unlike CLICK A, which will use an oscilloscope to sample the OGS APD data, during the B/C mission, the demodulation electronics developed for the B/C payloads will also be used by the ground station to demodulate the communications signal in real-time.

1.1 Crosslink Analysis

Although crosslinks between spacecraft in a string-of-pearls configuration do not have the rapidly varying range challenges of a downlink, they do have a stray light control challenge since the sun can easily come within the keep out angle of the payload sensors. To mitigate this, the CLICK B/C payloads are designed with stray light control features and coatings to mitigate noise from solar radiation up to a keep out half angle of 46.5° (see Section 2).

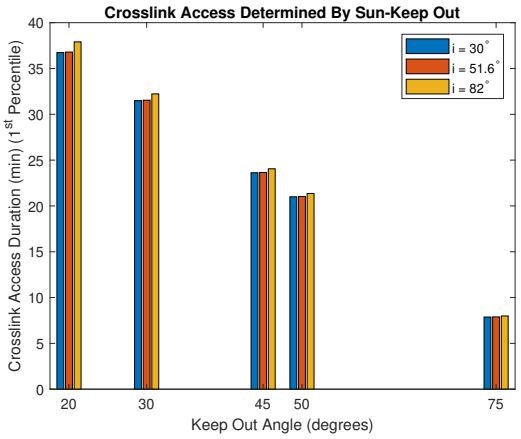

Figure 2: Crosslink access durations as determined by various Sun keep-out angles. The statistic plotted is the 1st percentile of the data aggregated, which means that 99% of the access intervals are greater than this value. The orbits computed are near-circular (e = 0.005) at 500 km altitude over three different inclinations (the results for 400 km and 600 km are not significantly different). Figure re-produced here with permission from Grenfell.[2]

To see the impact of this on operations, a crosslink access analysis was carried out using AGI's System's Tool Kit (STK) in a previous work of one of the authors.[2] The results are re-produced in Figure 2, which shows that for the payload's keep out angle, the crosslink access duration is greater than 21 minutes for 99% of crosslink access intervals, which is more than sufficient to meet the maximum experiment duration of 17 minutes (up to a 15 minute beacon link plus up to 2 minutes pre-beacon-link).

Table 1 shows the link budgets for the crosslink experiment at the minimum and maximum required ranges of 25 km and 580 km, respectively. The fixed parameters are determined by the terminal parameters: transmit power (P_{Tx}), transmit gain (G_{Tx}), receive gain (G_{Rx}), and transmitter and receiver implementation losses ($L_{\mathrm{Tx,imp}}$ & $L_{\mathrm{Rx,imp}}$). The transmit gain is set by the divergence of laser, which also contributes to the pointing loss. Simultaneous optimization of transmit gain and pointing loss is discussed in detail for the CLICK A OGS beacon in Cierny et al.[1] and briefly discussed further in the context of the CLICK B/C crosslink beacon in Section 1.2. The implementation losses are estimated from optical coatings and fiber losses. All requirement metrics are met at the required ranges with margin. In particular, the primary mission requirement of $\geq$ 20 Mbps is met using pulse position modulation (PPM) order 16, which has a data rate of 21.5 Mbps. A step-by-step discussion of the analysis involved in computing each link term is beyond the scope of this work; however, further discussion of the equations used for each link budget term can be found in Grenfell,[2] Casey & Lambert,[3] Clements,[4] Clements et al.,[5] and Kingsbury.[6]

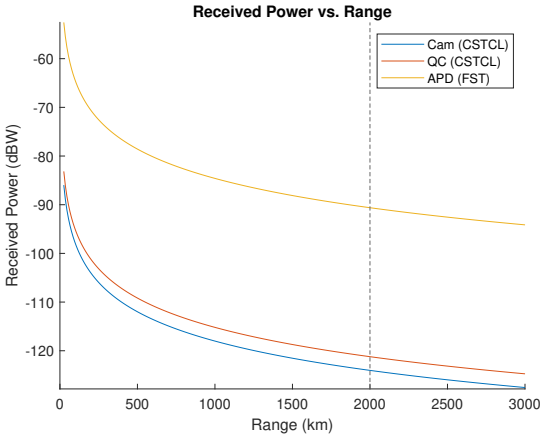

Figure 3: Received sensor power over various ranges.

Figure 3 shows the received power (P_{Rx}) for all three payload sensors as a function of the link range. For simplicity, the CSTCL mode is used for the pointing loss in the camera link budget, which yields the same pointing loss as that used for the quad-cell in Table 1. A comprehensive survey of pointing loss versus range for the CSTOL mode is beyond the scope of this work; however, details on the fu-

ture work needed for this can be found in Grenfell.[2] Looking at the pointing loss values for the quadcell from Table 1, it is apparent that range variation between 25 km and 580 km is negligible for pointing error, which will be discussed further in Section 1.2. For now, it is enough to note that the variation in received power is dominated by the variation in path loss (L_{path}) as a function of range, with a variation in path loss of 27.3 dB for the 555 km variation in range from 25 km to 580 km.

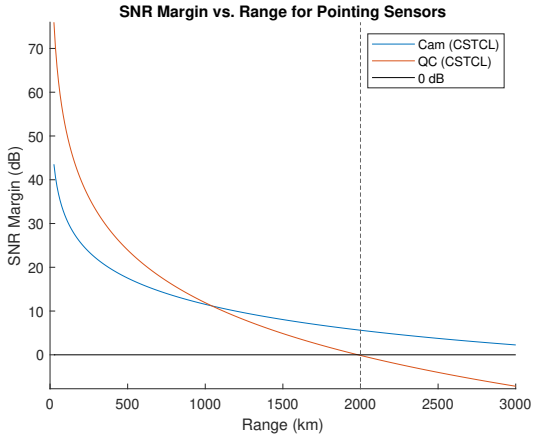

Figure 4: Pointing sensor SNR margins over various ranges.

Figure 4 gives the SNR margins for the pointing sensors (the quadcell and the camera) with respect to range variations. The CSTCL pointing mode is used again. The limiting sensor is the quadcell, which maintains a 0 dB performance margin up to a maximum range of 2000 km given the link parameters. For missions working with longer ranges, a narrower divergence beacon would be a straightforward modification since the beacon divergence used here is governed by the open-loop pointing performance at the minimum mission range of 25 km (see Section 1.2). This is because the open-loop pointing performance improves with increased range, since a dominant effect in open-loop pointing is the relative navigation error: the ratio of the angular relative error in the estimated S/C positions to the range. A practical point for the CLICK B/C mission is that the crosslink radio is designed for the 25 km to 580 km mission ranges is unlikely to be useful for extended mission testing at longer ranges. It is possible that open-loop pointing of the spacecraft even with relatively old (e.g. up to 24 hours) ephemeris data provided by the MOC would be sufficient to close the beacon link at sufficiently long ranges, either by direct open-loop pointing or by utilizing a scanning maneuver. Further discussion of this can be found in Grenfell;[2] however, detailed analysis of this off-nominal operational mode is future work.

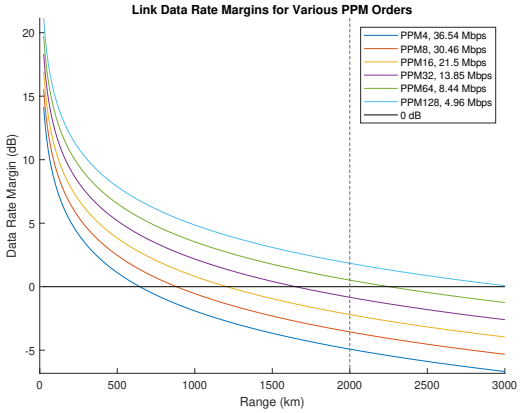

Figure 5: Data rate margins over various ranges for various PPM orders.

Figure 5 shows the variation in data rate margin as a function of crosslink range for various PPM orders. The lower PPM orders have higher data rates and more stringent power requirements; and hence, lower margins. The limiting range of 2000 km for the quadcell sensor is illustrated with a vertical dashed line. Ignoring the quadcell limitation for the sake of argument, the maximum communications ranges and nominal data transfer amounts are given in Table 7. Even with PPM4, the communications link has margin out to 645.0 km, well beyond the maximum required link range of 580 km. A PPM16, 21.5 Mbps link can be maintained up to 1206.6 km, and a PPM128, 4.96 Mbps link can be maintained up to 3056.9 km. As in the case of the beacon, even longer ranges would be possible with a narrower transmit divergence, the pointing challenges of which are discussed in the next section.

Table 2: Crosslink communications metrics for various PPM orders.

PPM	Data Rate (Mbps)	Max Range (km)	Data Transfer (Gb)
4	36.54	645.0	10.96 - 30.70
8	30.46	881.8	9.14 - 25.58
16	21.5	1206.6	6.45 - 18.06
32	13.85	1650.8	4.15 - 11.63
64	8.44	2253.2	2.53 - 7.09
128	4.96	3056.9	1.49 - 4.17

Transfer amounts are for link durations of 5 - 14 min.

In this section, the potential duration of the crosslink experiment was determined to be greater than 21 minutes for 99% of link access intervals under the constraint 46.5° sun keep out half-angle of the camera baffle. This easily accommodates the planned experiment durations of up to 17 minutes;

Table 1: Crosslink experiment link budgets at the minimum and maximum ranges.

Link Parameter	APD		Quadcell		Camera	
P_{Tx} (dBW)	-6.99	200 mW avg.	-6.02	2.5 W avg.	-6.02	2.5 W avg.
G_{Tx} (dB)	93.40	121 μrad $1/e^2$	57.97	7147 μrad $1/e^2$	57.97	7147 μrad $1/e^2$
G_{Rx} (dB)	93.32	22.86 mm Ap.	97.35	22.86 mm Ap.	-94.48	16.4 mm Ap.
L_{path} (dB)	-226.1, -253.4	25 km, 580 km	-230.2, -257.5	25 km, 580 km	-230.2, -257.5	25 km, 580 km
$L_{\text{Tx,imp}}$ (dB)	-1.55	CBE	-1.02	CBE	-1.02	CBE
$L_{\text{Rx,imp}}$ (dB)	-0.86	CBE	-1.15	CBE	-1.10	CBE
L_{ptg} (dB) (99.7%)	-3.51, -3.73	38.1 μrad, 39.3 μrad	-0.12, -0.12	417 μrad, 418 μrad	-4.34, -3.41	2527 μrad, 2238 μrad
P_{Rx} (dBW)	-52.33, -79.86		-83.16, -110.5		-90.20, -116.6	
$P_{\text{Rx,bkgd}}$ (dBW)	-222.6	eclipse	-217.4	eclipse	-207.1	eclipse
Metric	-52.33, -79.86	P_{Rx} (dBW)	85.82, 31.20	SNR (dB)	48.80, 22.45	SNR (dB)
Requirement (dB)	-69.38, -83.05	P_{req} - PPM16	9.83	SNR_{req}	9.48	SNR_{req}
Margin (dB)	17.06, 3.18		75.98, 21.36		39.32, 12.97	

APD ranging SNR values: 31.82 dB at 25 km, 16.08 dB at 580 km. 1537 nm or 1563 nm Tx to APD. Using 1550 nm avg. here for simplicity. 974 nm Beacon to quadcell and camera.

therefore, the camera baffle design, which will be discussed in Section 2, is sufficient for the CLICK B/C mission. Next, link analysis showed that the primary mission requirement of $\geq$ 20 Mbps at ranges of 25 km and 580 km is met using pulse position modulation (PPM) order 16, which has a data rate of 21.5 Mbps. Furthermore, for the time-transfer ranging capability, SNR values of 31.82 dB and 16.08 dB were found for 25 km and 580 km. Moreover, it was found that the quadcell SNR margin limits the payload's maximum crosslink range to less than 2000 km. Lastly, PPM orders between 4 and 128 were compared; and with a PPM 4, a 35.54 Mbps communications link can be maintained out to 645.0 km with potential data transfers of 10.96 - 30.70 Gb for link durations of 5 - 14 minutes. Furthermore, given a PPM order of 32, a 13.85 Mbps communications link can be maintained out to 1650.8 km with potential data transfers of 4.15 - 11.63 Gb for the same link durations.

1.2 Crosslink Pointing Budgets

There are three separate laser pointing budgets that are used to analyze pointing loss for the crosslink experiment link budgets. The pointing budgets for the beacon laser when operating in open-loop (CSTOL) and closed-loop (CSTCL) coarse stage tracking modes are given in Tables 3 & 4, respectively. The pointing budget for the payload laser during fine stage tracking (FST) is given in Table 5. In these tables, $\Theta_{\text{ptg}} = \sqrt{\Theta_x^2 + \Theta_y^2} \sim \text{Rice}(\sqrt{2}\mu, \sigma)$ is the total two-axis pointing error, with μ and σ being the Gaussian parameters of the sum of the single axis pointing error components: $\Theta_x \sim N(\mu, \sigma)$ & $\Theta_y \sim N(\mu, \sigma)$. These are conservatively modeled as symmetric Gaussian random variables by using the worst case axial pointing error component when geometric asymmetries are present in the error components. The reader is referred to Grenfell[2] for an in-depth discussion and derivation of the statistical pointing error and loss models used here.

In Table 3, the pointing error and loss for the beacon laser is given for open-loop S/C bus pointing (CSTOL), which utilizes ephemeris data for both spacecraft derived from their onboard GPS receivers and exchanged over the RF crosslink at the beginning of the crosslink experiment. The analysis of the relative navigation error associated with this process can be found in Grenfell,[2] and the values from this reference are used here.

Point ahead error is the error associated with the finite speed of light, similar to how the finite speed of any projectile must be taken into account when attempting to hit a target. The formula for

point ahead error in open-loop is $\theta_{\text{PA}} = v_{\text{rel,perp}}/c$, where $v_{\text{rel,perp}}$ is the magnitude of the component of the relative velocity between the transmitter and the receiver that is orthogonal to the line of sight. In closed-loop, this error doubles because there is a contribution from the target's laser signal in addition to the transmitter's laser signal. The values used here are based on previous a statistical analysis of point ahead error for LEO orbit downlinks.[2]

Table 3: Pointing error budget for crosslink coarse stage tracking in open-loop at minimum & maximum ranges.

Budget Element	25 km range		580 km range	
	μ (μrad)	σ (μrad)	μ (μrad)	σ (μrad)
Relative Navigation	13.80	343.1	0.001	20.44
Open-Loop Point Ahead	0.063	0.001	1.46	0.016
P/L Fiducial Msmt. Residual	0	484.8	0	484.8
Launch Induced Shift	0	423.3	0	423.3
Thermal Deformation	38.15	4.36	38.15	4.36
Spacecraft Body Pointing	0	122.2	0	122.2
Total	52.02	739.5	39.61	655.5
θ_{1/e^2} [μrad]	7147			
θ_{ptg} [μrad] ($p_\theta = 0.997$)	2527		2238	
$L_{\text{ptg,dB}}$ [dB] ($p_l = 0.997$)	-4.343		-3.407	

The payload (P/L) fiducial measurement residual error comes from the measurement residual of the offset between the payload fiducial mirror and the S/C star tracker fiducial mirror, which is input to the attitude pointing commands to compensate for the offset. This measurement is carried out using theodolites during AI&T of the payload and the spacecraft.

The launch-induced shift is the possible displacement of the beacon mount relative to the star tracker frame due to launch vibrations. Due to the nature of root-square-sum errors (the "weak link" dominates the error budget), the best way to estimate this value a priori is to simply analyze the worst potential offender, which for the B/C payload is the shift of the optical bench relative to the payload structure (see Figures 10 & 12). The value used here is an estimate based on the mounting feature geometry and 0.001" tolerances for the thermal spacers used at the interface between the optical bench and the EDFA plate (the structural component the optical bench is mounted to). This value will be verified during environmental testing of the B/C payload; however, there is the potential for additional launch-shift error contributions associated with the integrated spacecraft and not just the payload. Therefore, the CLICK A mission serves an important role of risk-reduction for this error estimate because it will not be known with high certainty how the entire integrated spacecraft behaves under vibration until AI&T, which is too late in the development process to change the B/C beacon divergence if errors that are significantly larger than anticipated are found. Therefore, measurements of launch shift during AI&T of the CLICK A payload will be useful for determining the best divergence angle for the B/C payload beacon.

The next error term is due to thermal deformation of the spacecraft bus that causes an error offset between the beacon and the star tracker. This error values used here come from the analysis found in Yenchesky et al.[7] Lastly, the spacecraft body pointing error is the error associated with the spacecraft's attitude determination and control system. The value used here is based on previous mission performance of the Blue Canyon Technologies (BCT) spacecraft bus.[8]

A final point of note concerning the CSTOL pointing budget is the beacon divergence angle. The design value used is based on the estimated CSTOL error distribution at 25 km, $N(52.02, 739.5)\mu$rad, which is the worst case pointing distribution for the beacon during PAT due to the inverse relationship between relative navigation performance and range. A useful fact about link budget analysis is that the combined transmit gain and pointing loss ($G_{\text{Tx}} + L_{\text{ptg}}$) has a global maximum at a particular divergence value. This can be determined by analysis of the statistical pointing loss model given the error distribution, $N(\mu, \sigma)$, according to Equation 1.[1]

$$\theta^*_{1/e^2} = \sqrt{8\sigma^2 F_X^{-1}(p_r; \mu, \sigma)} \tag{1}$$

where $X \sim \chi^2_2(2\mu^2/\sigma^2)$ (i.e. a noncentral chi-squared distribution with two degrees of freedom),[2] and $F_X^{-1}(p_r; \mu, \sigma)$ is the inverse cumulative distribution function of this distribution, evaluated numerically using the pointing error distribution parameters. See Cierny et al.[1] for a useful analytical approximation to the numerical solution for case of small bias errors ($\mu/\sigma \approx 0$). If one plugs the optimal divergence value into the pointing loss model,[1,2] the optimal pointing loss is $L^*_{\text{ptg,dB}}(\theta^*_{1/e^2}) = -10\log_{10}(e) \approx -4.343$ dB. Since the beacon is optimized for CSTOL at 25 km, this is the value of the pointing loss for this mode found

in Table 3.

Table 4 gives the beacon pointing error budget for closed-loop spacecraft pointing using 1 Hz feedback of error angle data generated by centroid measurements of the received beacon spot on the camera. Now the relative navigation error from open-loop is replaced with the error associated with this sensor measurement, which is quantified in the budget by the noise equivalent angle (NEA). The formula for this is NEA $= 1/(\text{SF} * \sqrt{\text{SNR}})$, where SF is the slope factor of the sensor, which for a Gaussian spot is given as SF $= 1.56/\theta_{\text{spot}}$.[3] θ_{spot} is the angular size of the spot, which is computed based on the radius of the first minimum of an Airy disk: $\theta_{\text{spot}} = 2.44\lambda F\#/f$.[3]

Table 4: Pointing error budget for crosslink coarse stage tracking in closed-loop at minimum & maximum ranges.

Budget Element	25 km range		580 km range	
	μ (μrad)	σ (μrad)	μ (μrad)	σ (μrad)
Camera NEA	0	0.337	0	7.00
Closed-Loop Point Ahead	0.126	0.001	2.911	0.031
Camera feedback calibration residual	0	3.98	0	3.98
Beacon-to-Camera calibration residual	0	2.95	0	2.95
Spacecraft Body Pointing	0	122.2	0	122.2
Total	0.126	122.3	2.911	122.5
θ_{1/e^2} [μrad]	7147			
θ_{ptg} [μrad] ($p_\theta = 0.997$)	416.8		417.6	
$L_{\text{ptg,dB}}$ [dB] ($p_l = 0.997$)	-0.1181		-0.1186	

As previously mentioned, the point ahead error in closed-loop is twice that used in Table 3. The camera feedback calibration residual is an estimate of the error residual associated with calibrating the relationship between centroid measurements and error angles. The model used in the software is a simple linear model relating the centroid coordinate to the angle coordinate: $x_c = f_x\theta_x + c_x$, $y_c = f_y\theta_y + c_y$, where (x_c, y_c) is the centroid coordinate, (f_x, f_y) are the effective focal lengths in each axis (asymmetries can exist due to hardware defects and unmodeled distortion effects e.g. radial and tangential distortions), and (c_x, c_y) is a centroid bias offset. Hardware testing of this calibration method is in-progress, and the value used here is a combination of an experimental result for the centroiding accuracy of the camera (2.32μrad 1-σ) and an estimate for the in-development calibration rig mechanical setting resolution based on the quoted hardware accuracy (3.23μrad 1-σ).

The beacon-to-camera calibration residual error is also an estimate via the combination of two errors. The first is the measurement residual of the misalignment between the camera and quadcell, which is given by the centroiding accuracy of the camera (2.32μrad 1-σ). The second is the calibration residual error between the beacon laser and the quadcell, which is given by the centroiding accuracy of the quadcell (1.83μrad 1-σ), which will now be discussed further in the context of the fine stage tracking (FST) pointing budget.

Table 10 gives the transmit laser pointing error for fine stage tracking using closed-loop feedback from the quadcell to the FSM. The first element of error is therefore given by the NEA of the quadcell. The value used here is somewhat larger than the value that would be calculated using the formulas previously discussed in the context of the camera. This is because the formula for the slope factor assumes that the loss in the gaps between sensor pixels is negligible; however, for the quadcell, the gap does cause losses that are significant for the analysis. Therefore, in order to estimate the NEA for the quadcell, a Zemax model of its the point spread function is used to find the given value (see Table 11).

Table 5: Pointing error budget for crosslink fine stage tracking at minimum & maximum ranges.

Budget Element	25 km range		580 km range	
	μ (μrad)	σ (μrad)	μ (μrad)	σ (μrad)
Quadcell NEA	0	1.826	0	1.826
FSM Control Residual	0.062	3.077	0.062	3.077
Closed-Loop Point Ahead	0.126	0.001	2.911	0.031
Tx-to-Quadcell alignment residual	0	9.178	0	9.178
Thermal Deformation	0	5.396	0	5.396
S/C Reaction Wheel Jitter	0	1.454	0	1.454
Total	0.188	11.27	2.973	11.27
θ_{1/e^2} [μrad]	121.0			
θ_{ptg} [μrad] ($p_\theta = 0.997$)	38.42		39.66	
$L_{\text{ptg,dB}}$ [dB] ($p_l = 0.997$)	-3.506		-3.734	

The next error is the error associated with control of the FSM, which is an experimental result using the flat satellite development board. This value will be further refined during EDU testing. The Tx-to-Quadcell alignment residual is the error associ-

ated with kinematic adjustment of the Tx collimator with respect to the quadcell boresight. The error value used here is an estimate of the measurement residual of the calibration rig that will be used during EDU assembly and alignment.

The thermal deformation value used is based on a preliminary finite element analysis (FEA) of the payload optical bench alone, which is the largest element and therefore subject to the greatest thermal deformations (thermoelastic expansion effects are proportional to the initial size of the part). A more detailed FEA of the payload optical bench will be carried out as part of future work using the thermal models detailed in Section 4.

Lastly, the jitter term comes from the spacecraft's reaction wheels, which are running throughout the experiment in order for the spacecraft bus to point the payload apertures at the target. The estimate here is based on results from ASTERIA, which also used a BCT bus, with a factor of safety of 3.[9] The $1/e^2$ divergence value used for the transmit laser was set at the beginning of mission development, and despite improved error estimates is still close to the optimal value for the 580 km FST budget, which using using Equation 1 is currently 112. μrad given the $N(2.973, 11.27)\mu$rad error distribution. All of the fine stage tracking error values except for point ahead (which is purely determined by the orbital dynamics) will be tested during AI&T for the EDU and the S/C.

In this section, the pointing budget analysis for crosslink beacon laser when operating in open-loop (CSTOL) and closed-loop (CSTCL) coarse stage tracking modes are given as well as the pointing budget for the transmit laser operating in fine stage tracking (FST) mode. The 7147μrad $1/e^2$ (0.24° full-width at half-maximum (FWHM)) crosslink beacon divergence coupled with open-loop and closed-loop 3σ pointing errors of 2527 to 2238μrad and 416.8 to 417.6μrad yielded pointing losses of -4.343 to -3.407 dB and -0.1181 to -0.1186 dB for the mission ranges of 25 to 580 km, respectively. The 121.0μrad $1/e^2$ (71.2μrad FWHM) transmit laser divergence coupled with a closed-loop 3σ pointing error of 38.42 to 39.66μrad yielded pointing losses of -3.506 to -3.734 dB for the mission ranges of 25 to 580 km. These pointing loss values are sufficient for the beacon and communications crosslinks as discussed in Section 1.1.

1.3 Downlink Analysis

In this section, the analysis of a downlink experiment using the CLICK B/C payload will be presented. Optical downlink experiments will be performed using an optical ground station (OGS) located at MIT Wallace Astrophysical Observatory. The OGS is called the Portable Telescope for Lasercom (PorTeL), which is described in detail in other references.[10,11] This section will follow the approach for the analysis of the CLICK A downlink experiment, which is presented in detail in Cierny et al.[1] A reference downlink overpass is selected from a survey of low Earth orbit overpasses given a nominal orbit consistent with the International Space Station (ISS) (the CLICK A payload is being deployed from the ISS). A comprehensive survey of link analysis variations with different orbits is future work requiring further optimization for run-times of the link analysis software used. The reference overpass is selected based on an overpass survey analysis carried out using AGI's System's Tool Kit (STK), the details of which are described in Cierny et al.[1] The reference pass epoch is July 09, 2021 at 03:52:15.000 UTC, with the following orbital elements at epoch: $(a = 6791.3\text{km}, e = 6.084 * 10^{-4}, i = 51.483°, \Omega = 221.52°, \omega_p = 181.99°, M = 220.44°)$.[1] The pass duration is 10.90 minutes, the maximum pass elevation is 53.99°, the minimum pass range is 517.60 km, and the pass occurs during eclipse of the OGS.[1]

The link budget parameters for the three link sensors (OGS-APD, OGS-Camera, S/C-Quadcell) are given at the minimum pass range in Table 6, and the variations of the most important link parameters during the pass are given in Figures 6 - 9. Table 6 shows the fixed link parameters as well as the variable link parameters captured at minimum range. The fixed parameters include the transmitter implementation loss ($L_{\text{Tx,imp}}$) and the receiver implementation loss ($L_{\text{Rx,imp}}$), which are both computed based on optical coating and fiber losses in the relevant optical trains. The margin associated with PPM32 is given here since this is the maximum PPM order that enables a $\geq$ 10 Mbps downlink to satisfy the mission requirement. Additional results with other PPM orders are shown in Figure 9 and Table 7. A step-by-step discussion of the analysis involved in computing each link term is beyond the scope of this work; however, further discussion of the equations used for each link budget term can be found in Grenfell,[2] Casey & Lambert,[3] Clements,[4] Clements et al.,[5] and Kingsbury.[6]

Figure 6 shows the received power for each of the three sensors over the duration of the pass as well as the link ranges during the pass. The received power for the OGS sensors are restricted to the time period defined by closed loop tracking of the downlink laser, which begins simultaneously with the closure of the

Table 6: Downlink experiment link budgets at the minimum range of the reference overpass.

Link Parameter	OGS-APD		OGS-Camera		S/C-Quadcell	
P_{Tx} (dBW)	-6.99	200 mW avg.	-6.99	200 mW avg.	3.98	2.5 W avg.
G_{Tx} (dB)	93.40	121 μrad $1/e^2$	93.40	121 μrad $1/e^2$	55.51	9487 μrad $1/e^2$
G_{Rx} (dB)	115.1	28 cm Aper.	115.1	28 cm Aper.	97.34	22.86 mm Ap.
L_{path} (dB)	-252.5	517.60 km	-252.5	517.60 km	-256.5	517.60 km
$L_{\mathrm{Tx,imp}}$ (dB)	-1.55	CBE	-1.55	CBE	-1.02	CBE
$L_{\mathrm{Rx,imp}}$ (dB)	-0.82	CBE	-11.27	CBE	-1.15	CBE
L_{ptg} (dB) (99.7%)	-14.49	78.1 μrad	-14.49	78.1 μrad	-0.04	304.7 μrad
L_{atm} (dB)	-2.10	el = 53.99°	-2.10	el = 53.99°	-2.10	el = 53.99°
P_{Rx} (dBW)	-60.92		-80.38		-104.0	
$P_{\mathrm{Rx,bkgd}}$ (dBW)	-181.6	eclipse	-169.0	eclipse	-208.5	eclipse
Metric	-60.92	P_{Rx} (dBW)	40.20	SNR (dB)	44.22	SNR (dB)
Requirement (dB)	-79.91	P_{req} - PPM16	8.25	$\mathrm{SNR}_{\mathrm{req}}$	9.62	$\mathrm{SNR}_{\mathrm{req}}$
Margin (dB)	9.99		31.95		34.39	

1537 nm or 1563 nm Tx to OGS-APD & OGS-Camera (1537 nm used here e.g. CLICK B downlink).
975 nm Beacon to S/C-Quadcell.

beacon uplink to the S/C camera at at a range of 1499.6 km, which occurs at 2.17 minutes. The uplink is lost when this range is reached again 9.25 minutes into the pass.

The pointing loss (L_{ptg}) on both the uplink and the downlink are also variable. The computation of pointing loss will be discussed in Section 1.4, and the behavior during the pass is given in Figure 7. The uplink pointing loss is due to mispointing error of the ground beacon laser by the OGS. The main error contribution during the initial uplink phase is due to ephemeris error, which as discussed previously is inversely proportional to the range; hence, the increase in pointing error as the range decreases. The abrupt change is the transition to closed-loop uplink pointing when the uplink, and therefore the downlink, closes. The closed loop error variation with range is small due to relatively insignificant changes in the OGS camera's NEA compared to the other errors in the OGS's CSTCL pointing budget (see Table 9.

The SNR margin criterion for link closure to the pointing sensors is given in Figure 8. The SNR increases as range decreases and received power increases. The intersection point of the 0 dB line with the S/C-Quadcell SNR margin defines the link closure time of 2.17 minutes. The SNR margin is computed as the difference between the SNR computed from the link budget and a theoretical SNR requirement for the peak power point on the sensor using Equations 2a - 2b.[12]

$$\mathrm{TNR} = \sqrt{-2\ln\left(\sqrt{3}\mathrm{FAR}/f\right)} \tag{2a}$$

$$\mathrm{SNR}_{\mathrm{req}} = \sqrt{2}\mathrm{erf}^{-1}\left(2P_d - 1\right) + \mathrm{TNR} \tag{2b}$$

TNR is the threshold-to-noise ratio computed as a function of the false-alarm rate (FAR [Hz]) and the sensor bandwidth (f [Hz]). Following the approach taken by Yura,[12] the FAR is set to $3.171 * 10^{-8}$ Hz, which is 1 per year. The bandwidth of the S/C quadcell is 100 Hz, and the bandwidth of the OGS camera is 0.5 Hz,[10] though these rates are adjustable by changing the camera's integration time setting. These correspond to TNRs of 8.15 dB and 7.53 dB, respectively. The detection probability (P_d) is set to 99.9%, which yields the SNR requirements given in Table 6.

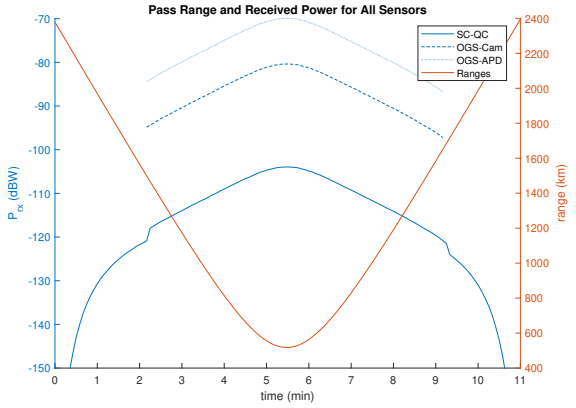

Figure 6: Link range and received power for all sensors for a reference overpass.

Finally, Figure 9 shows the range variation of margins for communications at various pulse-position-modulation (PPM) orders. Higher PPM orders have lower data rates (see the plot legend) and reduced requirements, which leads to higher margins. All PPM orders achieved positive margins dur-

ing the pass, including PPM orders of 32 or less, which are needed to achieve data rate ≥10 Mbps in order to satisfy the mission requirement. To get an idea of the amount of data it is theoretically possible to transfer with each of the PPM orders, the communications durations for each PPM order were computed.

The results are summarized in Table 7. The optimal PPM order for this pass would be PPM4 since it achieved the maximum data transfer of 12.42 Gb. A dynamic PPM would enable further optimization of data transfer. For example, if PPM order were to be adjusted to give the best available data rate throughout the pass, then the total data transfer would be 14.63 Gb.

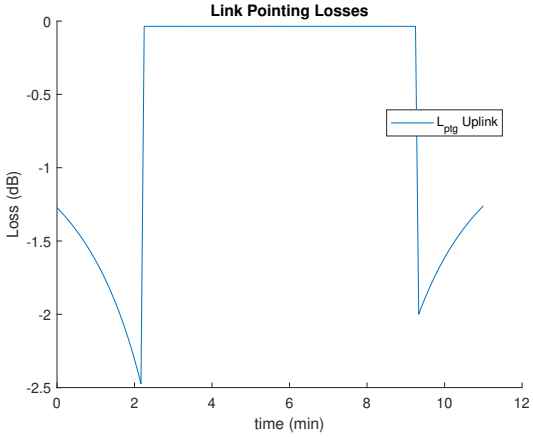

Figure 7: Link pointing losses for a reference overpass.

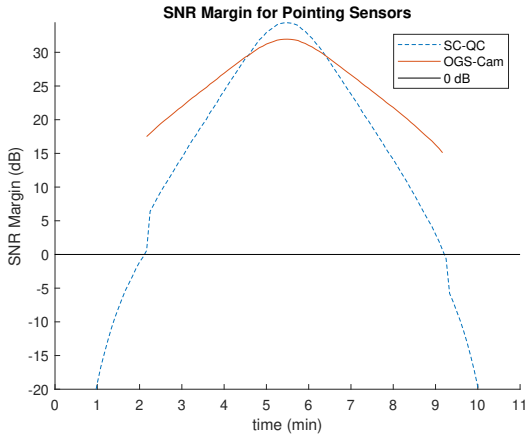

Figure 8: SNR margins for pointing sensors for a reference overpass.

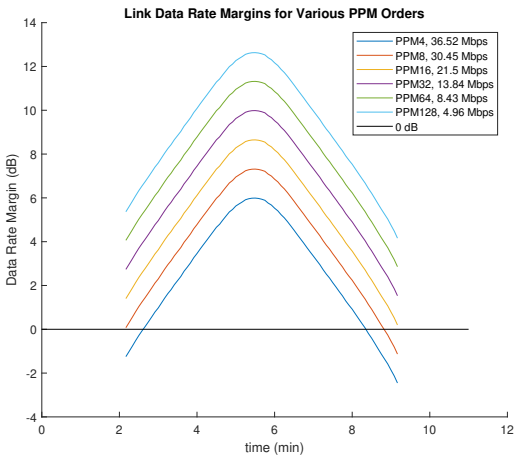

Figure 9: Downlink data rate margins for a reference overpass for various PPM orders.

Table 7: Communications metrics for a reference overpass.

PPM	Data Rate (Mbps)	Duration (s)	Data Transfer (Gb)
4	36.53	340	12.42
8	30.45	395	12.03
16	21.50	420	9.03
32	13.84	420	5.81
64	8.43	420	3.54
128	4.96	420	2.08

In this section, a single reference pass from a LEO ISS orbit was selected for link analysis from a survey of overpasses of the OGS location with the following characteristics: a pass duration was 10.90 minutes, maximum pass elevation of 53.99°, minimum pass range of 517.60 km, and occurring during eclipse of the OGS. Link analysis showed that the beacon uplink budgets closed for a duration of 7.08 minutes. Furthermore, all the communications downlink closed with margin for PPM orders 4 to 128 during the pass with respective durations between 5.7 minutes and 7 minutes. The mission requirement of ≥10 Mbps is satisfied for PPM orders less than 32. Furthermore, PPM 4 acheived the best theoretical data transfer of 12.42 Gb for a fixed PPM order. Lastly, an improved data transfer of 14.63 Gb could be achieved by optimal variation of the PPM order during the pass.

1.4 Downlink Pointing Budgets

There are three separate laser pointing budgets that are used to analyze pointing loss for the downlink experiment link budgets. The pointing budgets for the OGS beacon laser when operating in open-loop (CSTOL) and closed-loop (CSTCL) coarse stage

tracking modes are given in Tables 8 & 9, respectively. The pointing budget for the payload laser during fine stage tracking (FST) is given in Table 10.

Table 8: Pointing error budget for OGS beacon coarse stage tracking in open-loop (CSTOL) at time of uplink/downlink closure (1.67 min, 1699.8 km).

Budget Element	μ (μrad)	σ (μrad)
Satellite Ephemeris	0	517.5
OGS Star Tracker Calibration	0	315.1
Gimbal Pointing Jitter	0	85.11
Open-Loop Point Ahead	12.24	4.93
Beacon Alignment Residual	0	6.39
Total	12.24	611.9
θ_{1/e^2} (μrad)	9487	
θ_{ptg} (μrad, $p_\theta = 0.997$)	2086	
$L_{\text{ptg,dB}}$ (dB, $p_l = 0.997$)	-1.680	

Table 8 is nearly identical to the OGS CSTOL analysis used for the CLICK A analysis;[1] however, the acquisition time is later (2.17 minutes instead of 1.67 minutes), and therefore the range is shorter (1499.6 km instead of 1699.8 km).[1] This leads to larger satellite ephemeris error and thus a larger pointing loss (-1.680 dB instead of -1.414 dB);[1] however, this is not a significant enough difference to warrant changing the planned OGS divergence angle for the B/C pass at this time. The remaining error budget elements are described in the CLICK A analysis in Cierny et al.[1]

Table 9: Pointing error budget for OGS beacon coarse stage tracking in closed-loop (CSTCL) at time of uplink/downlink closure.

Budget Element	μ (μrad)	σ (μrad)
OGS Camera NEA	0	5.429
Gimbal Pointing Jitter	0	85.11
Closed-Loop Point Ahead	24.48	9.859
Beacon Alignment Residual	0	6.39
Total	12.24	86.09
θ_{1/e^2} (μrad)	9487	
θ_{ptg} (μrad, $p_\theta = 0.997$)	304.3	
$L_{\text{ptg,dB}}$ (dB, $p_l = 0.997$)	-0.036	

Table 9 is also nearly identical to the OGS CSTCL analysis used for the CLICK A analysis;[1] however, due to the higher gain transmit laser signal and the reduced range, the OGS camera NEA is reduced from 26.88μrad to 5.429μrad; however, due to the dominance of the jitter in the budget, this change does not significantly effect the pointing loss (improvement of 0.003 dB).[1]

Table 10 gives the pointing error model for the fine stage tracking (FST) using closed-loop FSM control via quadcell feedback. This analysis is nearly identical to the crosslink FST pointing budget (Table 5); however, there is now a significant point ahead error due to the significantly higher relative velocities involved in an overpass. Since the point ahead error is a significant fraction of the beam divergence, it leads to a large pointing error; however, due to the high transmit gain of the CLICK B/C laser and the high receiver gain of the OGS telescope, this loss is acceptable for the link budgets (see Section 1.3). Therefore, no compensation via the addition of a point ahead mirror (PAM) to the optical design or biasing the quadcell setpoint is necessary.

Table 10: Pointing error budget for payload fine stage tracking at time of uplink/downlink closure.

Budget Element	μ (μrad)	σ (μrad)
S/C Quadcell NEA	0	1.826
FSM Control Residual	0.062	3.077
Closed-Loop Point Ahead	24.48	9.859
Tx-to-Quadcell alignment residual	0	9.178
Thermal Deformation	0	5.396
Bus Reaction Wheel Jitter	0	1.45
Total	24.54	15.02
θ_{1/e^2} (μrad)	121.0	
θ_{ptg} (μrad, $p_\theta = 0.997$)	78.10	
$L_{\text{ptg,dB}}$ (dB, $p_l = 0.997$)	-14.49	

Finally, there are also analyses to determine the probability of acquisition given the field of view (FOV) of the three downlink sensors. For brevity, the tables associated with these analyses are omitted as the FOV's are all sufficiently large to virtually guarantee acquisition given the magnitudes of errors described in the pointing budgets.

The OGS camera has an FOV of $\pm 3484\mu$rad and a single-axis aperture open-loop tracking pointing error distributed as $N(0, 611.8)\mu$rad, which yields an acquisition probability at the time of downlink closure of 100% when rounded for significant figures. The OGS APD has an FOV of $\pm 217.9\mu$rad with an associated closed-loop tracking pointing distribution of $N(0, 19.23)\mu$rad, which also yields an acquisition probability of 100%.

The S/C quadcell has an FOV of $\pm 3142\mu$rad and an associated aperture pointing distribution of $N(38.15, 655.2)\mu$rad, which again yields an acquisition probability at the time of uplink closure of 100%. The quadcell's aperture pointing error consists of errors from onboard relative navigation ($N(0, 2.674)\mu\text{rad}^2$), measurement error of the misalignment between the payload fiducial and the spacecraft's star tracker fiducial ($N(0, 484.8)\mu$rad), error due to launch-induced shifts of the optical bench ($N(0, 423.3)\mu$rad), the error associ-

ated with the spacecraft's attitude control system ($N(0, 122.2)\mu$rad[8]), and the alignment error of the quadcell relative to the payload fiducial ($N(0, 7.816)\mu$rad). The notable reduction in alignment error of the quadcell relative to the fiducial as compared to the CLICK A camera alignment relative to the fiducial ($N(0, 2034)\mu$rad[1]). This is due to the implementation of kinematic mounts in the CLICK B/C optical train: the fiducial is mounted together with the beacon laser on a kinematic mount that is adjusted such that the beacon is co-boresighted with the quadcell.

In this section, the pointing budget analysis for the OGS beacon laser when operating in open-loop (CSTOL) and closed-loop (CSTCL) coarse stage tracking modes are given as well as the pointing budget for the spacecraft transmit laser operating in fine stage tracking (FST) mode. The 9487μrad $1/e^2$ (0.32° FWHM) uplink beacon divergence coupled with open-loop and closed-loop 3σ pointing errors of 2086μrad and 304.3μrad yielded pointing losses of -1.680 dB and -0.036 dB at the time of uplink acquisition. Upon uplink acquisition, the 121.0μrad $1/e^2$ (71.2μrad FWHM) transmit laser divergence coupled with a closed-loop 3σ pointing error of 78.10μrad yielded a pointing loss of -14.49 dB at the time up uplink acquisition, which is also the time of downlink closure. These pointing loss values are sufficient for the beacon uplink and communications downlink as discussed in Section 1.3.

2 Payload Optomechanical Design Developments

In this section, optomechanical design developments for the CLICK B/C payload beyond the designs reported in previous publications (Long[13] and Yenchesky et al.[7]) are summarized. The current payload design and its optical bench layout can be seen in Figure 12. The payload EDU is in the process of being manufactured for assembly and testing. Some of the optical bench components can be seen in Figure 10, which shows a fit check that was performed during manufacturing. The developments since the design reported in Yenchesky et al. include both minor and major design updates. Minor updates include cable and fiber routing in addition to the inclusion of detailed CAD for the electronics boards.

The first major update was the addition of a baffle for the camera, which, as discussed previously, was determined to be necessary to maximize available operations time by reducing the Sun keepout angle for the payload camera to 46.5° half-width. The available baffle length (24 mm) coupled with the camera lens diameter (18 mm) limits further reduction of this keep-out angle using the COTS camera lens assembly: the rear vane aperture diameter is set to 20.61 mm to maintain the 10.6° camera FOV, with the front vane aperture diameter then being set to 23.30 mm. Along with the front to rear vane distance of 20.83 mm, the minimum keep out angle is $\tan^{-1}((20.61+23.30)/(2*20.83)) = 46.5°$. It should be noted that if a custom camera lens assembly were to be built, a pinhole could be added between the refractive optics similar to the one included in the telescope (1 mm diameter pinhole), which would allow a significantly smaller keep-out angle while maintaining a similar form factor for improved crosslink access durations as shown in Figure 2. The geometry of the baffle vane gaps has been designed using specular baffle design theory, with 11 reflections for a ray incident from the outer edge of the baffle into the final vane gap prior to the lens. The coating applied to the baffle is Optical Black© by Pioneer Metal, with an absorptivity of $\sim 95\%$.[14] This gives an expected absorption with 11 reflections of -143.1 dB, which is used in the background power computation in the link analysis.

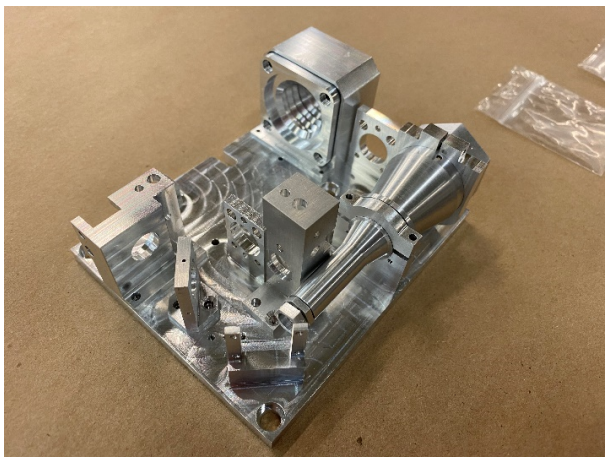

Figure 10: Fit check of parts for EDU optical bench during manufacturing.

It should be noted that the telescope components as well as the beam dump components (which includes the rear structural plate) are also coated with Optical Black©. Figure 14 shows the beam dump design as well as a bench top test of a 3D-printed prototype. The prototype used matte black plastic, which has poorer performance than the black coated aluminum, which will be used for the EDU (the test will be repeated with the EDU). Despite this, the beam dump performance was -31 dB absorption, which met the -30 dB requirement from the isolation budget. The primary source of stray

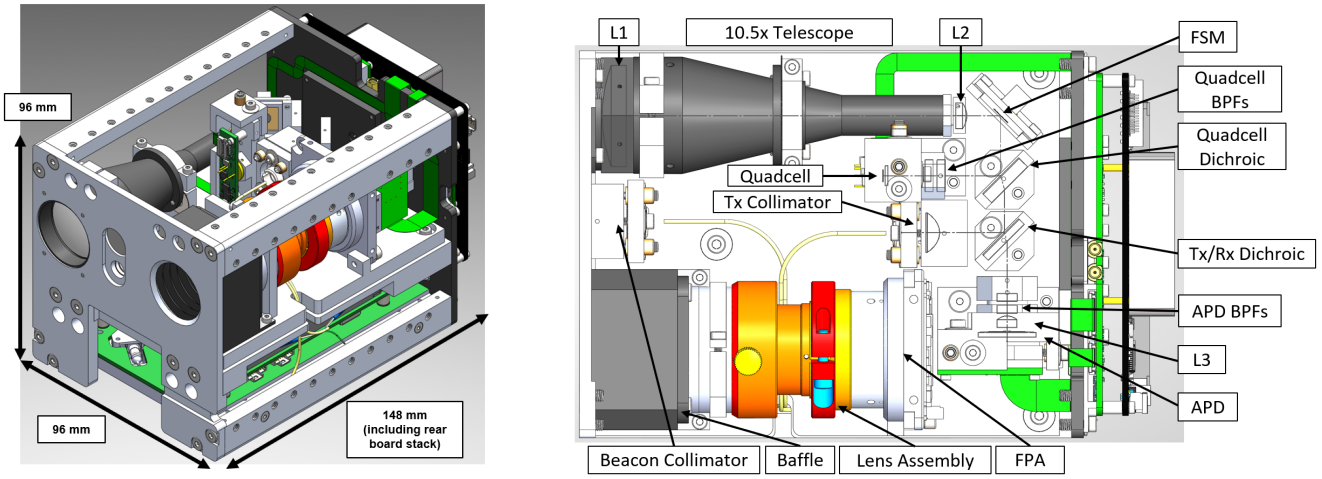

Figure 12: a) CLICK B/C Payload Isometric View. b) CLICK B/C Payload Optical Layout.

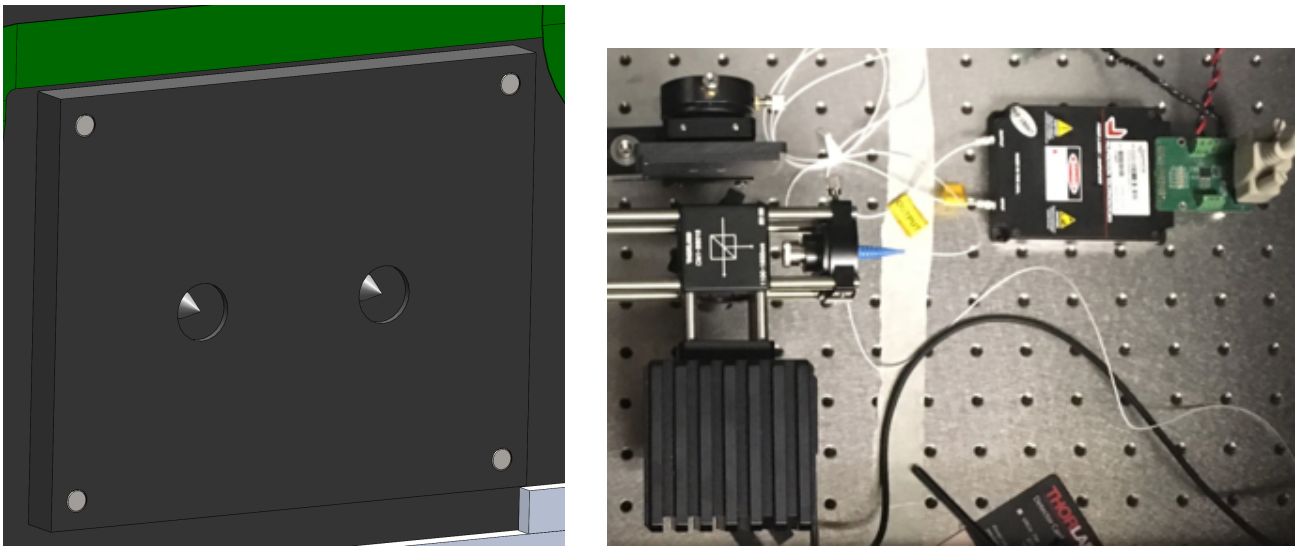

Figure 14: a) Beam Dump Design. Includes entry points for stray light reflected from both dichroics. b) Bench top test of 3D-printed beam dump prototype.

light of concern for the APD is the transmit laser. The Tx/Rx dichroic passes 5% of the transmit signal, which enters the beam dump. It should be noted however that this is not the main stray light path for the transmit laser, which is actually a 0.1% backreflection from the C-coated L2 telescope lens. In order to isolate the APD from this, two OD3 filters are placed in front of it that block the transmit beam, which give a combined attenuation of −60 dB. This, together with contributions from the dichroic and other optical elements along this path give a total attenuation of Tx stray light to the APD of −104.2 dB. Combining this path with the beam dump paths for stray light gives a total expected noise power at the APD due to Tx stray light of −108.2 dBW, sufficient for 28.34 dB of margin given the received signal power at 580 km of −79.86 dBW.

The second major update was an improvement in the fixturing design for the optical mounts, which are now based on a three part design for alignment and staking. An example of this for the quadcell dichroic mount is shown in Figure 15. This method is also used for the mounts for the Tx/Rx dichroic, quadcell, and APD. First, a press fit alignment pin is placed in the optic mount that aligns it with a hole in the optical bench. Next a countersunk screw is used to both secure the optic mount to the bench as well as provide an additional point of contact on the optical bench to constrain the mount from rotating about the alignment pin. Lastly, an oversized hole is placed in the mount where an additional staking pin is placed in the optical bench. This hole is filled with staking epoxy in order to prevent the mount from shifting under vibration.

Table 11: Quadcell Update Sensor Comparison

Specification	FirstSensor QP-6	Advanced Photonix SD085
Quadrant Gap	16 μm	10 μm
Noise Equivalent Angle (3σ)	19.5 μrad	5.5 μrad
Active Area	1 mm^2	9 mm^2
Field of View	±0.135°	±0.180°

A third update was a change in the part number for the quadcell sensor. This was motivated in part due to supplier issues with the previous part number in addition to improved performance for the new part number, which is summarized in Table 11.

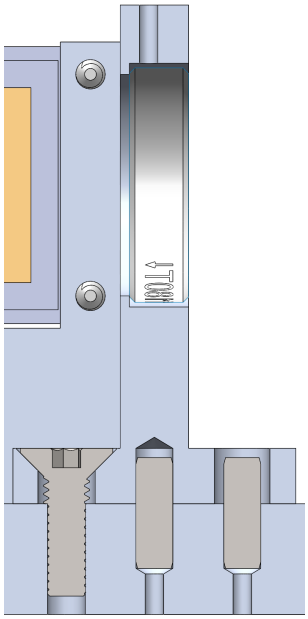

Figure 15: Optical Mount Fixturing Design Update

In this section, three major updates to the payload optomechanical design made since previous reports were described. First, a baffle was added in front of the camera, with a keep out half-angle of 46.5° and an expected attenuation of at least −143.1 dB for stray light outside the keep out zone. Second, the fixturing design for the optics was improved to use a three part design based on a press fit alignment pin, countersunk loading fastener, and a staking pin. The third update was the change in the part number for the quadcell, which improved its NEA from 19.5μrad (3σ) to 5.5μrad (3σ) due to a reduction in the gap size from 16μm to 10μm. The quadcell's FOV also increased from ±0.135° to ±0.180°.

3 Payload Optical Sensitivity Analysis

Each optic in the payload has 6 degrees of freedom (DOF) that are constrained by the optomechanical fixturing: decenter in X & Y, piston (Z), tip (rotation about X), tilt (rotation about Y), and roll (rotation about Z). The Z axis is the local axis through the center of the optic, Y is vertically up, and X completes the right handed set. Local displacements in each of these DOF can be applied in a Zemax model (Figure 16) of the optical train to analyze the optical performance impact of displacement errors due to machine tolerances and calibration residuals. This same method can be used to assess the impact of thermoelastic displacements given a thermal-structural finite-element analysis. The nominal ma-

chine tolerances for dimensions that are not critical to optical fixturing are 127 μm (0.005"). The machine tolerances for dimensions that are critical to optical fixturing are 25.4 μm (0.001"). All parts with critical dimensions are subject to an additional inspection step by the manufacturer, and all parts for the EDU have met or exceeded the required tolerances. The tolerances and known part geometries are used to estimate local optic displacements by hand-calculations. These results were compiled and fed into a Zemax model of the optical train for tolerancing sensitivity analysis. The analysis metrics were: Tx gain (dB), power lost in quadcell gap (dB), beacon PSF width (μm), and power lost from APD (dB).

The first analysis indicated that the sensitivity to telescope focus due to piston displacement of L2 was high; therefore, a locking nut was added to the L2 bezel to allow it to be positioned in piston. It is anticipated that better than 25.4 μm piston accuracy can be achieved using this method. This enables fine adjustment of the L2 piston position while measurements of transmit beam are taken with a beam profiler.

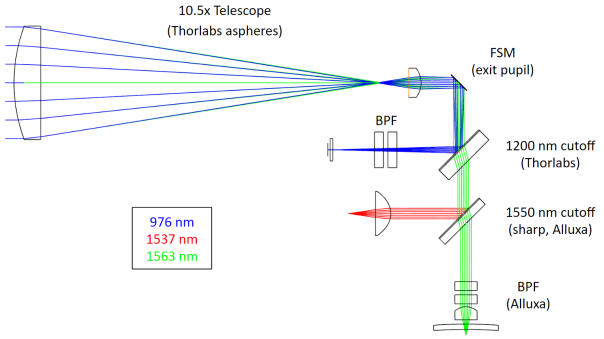

Figure 16: Zemax model ray trace for the payload optics.

For design efficiency, there is not a focusing lens for the quadcell sensor (this design decision is also described in Yenchesky et al.[7]). Rather, the 976 nm beam exiting the 1550 nm CWL telescope is not collimated and is converging. The quadcell is placed such that the path distance from the telescope L2 yields the desired spot size. A tolerancing analysis was done to determine the sensitivity of the estimated pointing loss induced by piston displacements. The results are shown in Figure 17. The quadcell position was calibrated within the available volume to about -1.7 dB gap loss (this is using the new 10 μm gap quadcell). This can be calibrated in-lab via a shim adjustment placed on the telescope tube, which can shift the entire telescope in piston by changing the height of a stack of 25.4 μm shims. Inspecting the graph, this is more than sufficient resolution for positioning to a negligible difference from the design gap loss.

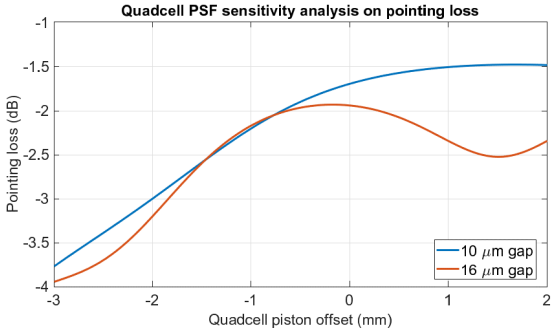

Figure 17: Quadcell piston sensitivity analysis results.

In this section, payload optical sensitivity results and design updates were summarized. Nominal machine tolerances are 127 μm (0.005") for non-critical dimensions and 25.4 μm (0.001") for critical dimensions. A Zemax model of the optical train for was used for tolerancing sensitivity analysis. This led to the addition of a kinematic adjustment in piston for L2, the elimination of the quadcell focusing lens, and the addition of a shim adjustment in piston for the telescope to adjust the quadcell spot size.

4 Payload Thermal Design Developments

The thermal model for CLICK-B/C payload design is based on the thermal model for the CLICK-A payload. The two payloads share many mechanical and thermal similarities, so both payloads were rebuilt together to standardize the methodology of how the models were built. Previously, the two payloads had different thermal model assumptions and techniques for simulating the heat loads that define the operation of the payload.

For the CLICK-B/C payload, the thermal subsystem is designed to be mostly passive, except for the heaters to get components up to operational temperatures during the cold case. The electronics for the CLICK BC payload use industrial grade electronic components whenever possible, due to their extended operational temperature range from -40°C to 85°C. The extended operating temperature range of the custom electronics assures the heater critical components will be able to turn on the payload heaters when necessary. A table of the survival and operational maximum and minimum temperatures is shown in Table 12. One particular component that was of concern was the mvBlueFOX-MLC205G-XOW-2111 camera since the manufactur-

ers data sheet has the lower operational temperature limit being 0°C. As discussed in the CLICK A paper, the camera was tested to a temperature -40°C to 40°C and operated as expected.

Table 12: Temperature Limits of Each Component

Component:	Temperature Limits of Each Component (°C)			
	Survival		Operational	
	Min	Max	Min	Max
Daughter Board	-55	125	-40	85
FPGA Board	-55	125	-40	85
APD Board	-55	125	-40	85
CPU Board	-55	85	-10	70
Optoelectronics Board	-55	125	-40	85
Quadcell Board	-55	125	-40	85
EDFA	-20	65	0	65
Camera	-40	60	-40	45

The thermal model for the CLICK BC payload was built from the CLICK A thermal model. Modifications were made to adjust to the difference in mechanical design from the two payloads. Namely, the separated optical bench and components as well as the the additional electronic boards on the back of the payload. The thermal model is built in Thermal Desktop (Cullimore and Ring Technologies). A picture of the thermal model next to the CAD model can be seen in Figure 18. The components of the payload can not be fully represented by the solid shapes that Thermal Desktop models are made of. Whenever possible, the geometry of components was modeled in the thermal model as it is in reality, but if the exact geometry could not be modeled, the correct thermal capacitance was modeled for all components.

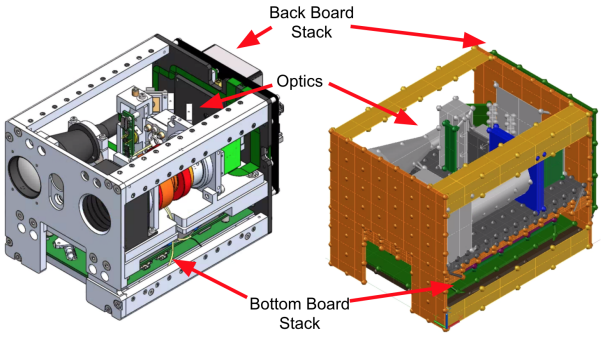

Figure 18: CAD Model Compared to Thermal Desktop Model

The CLICK-A and B/C payloads share a common mounting scheme for attaching the payload to the spacecraft. Since the bus provider is the same for both of the payloads, the thermal models of both payloads share similar boundary conditions. The boundary conditions of the model are time varying temperature defined nodes with the profile of the hot and cold boundary conditions provided by the bus provider. For now, the current transient temperature profile is the same as CLICK-A, but as the program develops and the bus provider is able to deliver CLICK-B/C specific boundary temperatures, the temperature profile will be updated. The interface between the payload and the spacecraft was defined between -10°C and 25°C. To model the heat loads, the team had to determine exactly what the concept of operations (CONOPs) would look like for a transmission. An outline of the modes that they payload goes through during a transmission is shown in Table 13.

Table 13: Heat Loads for Each Mode of Payload Crosslink Transmission

Component:	Power Draws (W) for Each Mode		
	Start Up (10 Minutes)	Transmit (15 Minutes)	Power Down (5 Minutes)
Daughter Board	1	5	1
FPGA Board	0	5.45	0
APD Board	0	2	0
CPU Board	2.53	2.84	2.53
Optoelectronics Board	0	6.39	0
EDFA	0	5.2	0
Camera	0	1	0
Heaters	10	0	0
Total	**13.53**	**27.88**	**3.53**

These modes define different heat loads for the power drawing components of the payload. These time dependent heat loads were input into the thermal model to assure that the temperatures that the components become during operation is within their operational temperature bounds. A 10°C margin was kept between all survival component temperature rating, to assure that the payload survives all thermal environments possible on orbit. The predicted temperatures of the components all maintain the margin outlined. The next step is build the EDU of the payload and run it through a TVAC test to determine the optical performance of the payload over a variety of temperatures.

In this section, the thermal model development for the CLICK B/C payload was described. The electronics used are industrial grade where possible, with an extended operational temperature range from -40°C to 85°C. The limiting components were the EDFA, with an operational temperature range of 0°C to 65°C, and the camera, with an operational

temperature range of -40°C to 45°C. The interface between the payload and the spacecraft was defined between -10°C and 25°C. The payload modes define different heat loads for the power drawing components. The thermal design maintains a 10°C margin from the survival temperature ratings of all components.

5 Conclusions and Future Work

The CubeSat Laser Infrared CrossLink (CLICK) mission goal is to demonstrate a low cost, high data rate optical transceiver terminal with fine pointing and precision time transfer in a *leq*1.5U form factor. There are two phases to the technology demonstration for the CLICK mission: CLICK-A downlink, and then CLICK-B/C crosslink and downlink. The topic of this paper is the design and prototyping of the laser communications (lasercom) terminal for the CLICK-B/C phase. CLICK B/C consists of two identical 3U CubeSats from Blue Canyon Technologies that will be launched together in Low Earth Orbit to demonstrate crosslinks at ranges between 25 km and 580 km with a data rate of $\geq$20 Mbps. Downlinks with data rates of $\geq$10 Mbps will also be demonstrated to the Portable Telescope for Lasercom (PorTeL) ground station.

Mission analysis showed that the potential duration of the crosslink experiment was determined to be greater than 21 minutes for 99% of link access intervals under the constraint 46.5° sun keep out half-angle of the camera baffle. This easily accommodates the planned experiment durations of up to 17 minutes; therefore, the camera baffle design, is sufficient for the CLICK B/C mission. Next, link analysis showed that the primary mission requirement of $\geq$ 20 Mbps at ranges of 25 km and 580 km is met using pulse position modulation (PPM) order 16, which has a data rate of 21.5 Mbps. Furthermore, for the time-transfer ranging capability, SNR values of 31.82 dB and 16.08 dB were found for 25 km and 580 km. Moreover, it was found that the quadcell SNR margin limits the payload's maximum crosslink range to less than 2000 km. Lastly, PPM orders between 4 and 128 were compared; and with a PPM 4, a 35.54 Mbps communications link can be maintained out to 645.0 km with potential data transfers of 10.96 - 30.70 Gb for link durations of 5 - 14 minutes. Furthermore, given a PPM order of 32, a 13.85 Mbps communications link can be maintained out to 1650.8 km with potential data transfers of 4.15 - 11.63 Gb for the same link durations.

Pointing budget analysis was presented for the crosslink beacon laser when operating in open-loop (CSTOL) and closed-loop (CSTCL) coarse stage tracking modes in addition to the transmit laser when operating in fine stage tracking (FST) mode. The 7147μrad $1/e^2$ (0.24° full-width at half-maximum (FWHM)) crosslink beacon divergence coupled with open-loop and closed-loop 3σ pointing errors of 2527 to 2238μrad and 416.8 to 417.6μrad yielded pointing losses of -4.343 to -3.407 dB and -0.1181 to -0.1186 dB for the mission ranges of 25 to 580 km, respectively. The 121.0μrad $1/e^2$ (71.2μrad FWHM) transmit laser divergence coupled with a closed-loop 3σ pointing error of 38.42 to 39.66μrad yielded pointing losses of -3.506 to -3.734 dB for the mission ranges of 25 to 580 km. These pointing loss values are sufficient for the beacon and communications crosslinks.

For downlink analysis, a single reference pass from a LEO ISS orbit was selected for link analysis from a survey of overpasses of the OGS location with the following characteristics: a pass duration was 10.90 minutes, maximum pass elevation of 53.99°, minimum pass range of 517.60 km, and occurring during eclipse of the OGS. Link analysis showed that the beacon uplink budgets closed for a duration of 7.08 minutes. Furthermore, all the communications downlink closed with margin for PPM orders 4 to 128 during the pass with respective durations between 5.7 minutes and 7 minutes. The mission requirement of $\geq$10 Mbps is satisfied for PPM orders less than 32. Furthermore, PPM 4 acheived the best theoretical data transfer of 12.42 Gb for a fixed PPM order. Lastly, an improved data transfer of 14.63 Gb could be achieved by optimal variation of the PPM order during the pass.

Pointing budget analysis was presented for the OGS beacon laser when operating in open-loop (CSTOL) and closed-loop (CSTCL) coarse stage tracking modes in addition to the spacecraft transmit laser operating in fine stage tracking (FST) mode. The 9487μrad $1/e^2$ (0.32° FWHM) uplink beacon divergence coupled with open-loop and closed-loop 3σ pointing errors of 2086μrad and 304.3μrad yielded pointing losses of -1.680 dB and -0.036 dB at the time of uplink acquisition. Upon uplink acquisition, the 121.0μrad $1/e^2$ (71.2μrad FWHM) transmit laser divergence coupled with a closed-loop 3σ pointing error of 78.10μrad yielded a pointing loss of -14.49 dB at the time up uplink acquisition, which is also the time of downlink closure. These pointing loss values are sufficient for the beacon uplink and communications downlink.

In addition to giving the status of payload EDU development, three major updates to the payload optomechanical design made since previous reports

were described. First, a baffle was added in front of the camera, with a keep out half-angle of 46.5° and an expected attenuation of at least −143.1 dB for stray light outside the keep out zone. Second, the fixturing design for the optics was improved to use a three part design based on a press fit alignment pin, countersunk loading fastener, and a staking pin. The third update was the change in the part number for the quadcell, which improved its NEA from 19.5μrad (3σ) to 5.5μrad (3σ) due to a reduction in the gap size from 16μm to 10μm. The quadcell's FOV also increased from $\pm 0.135°$ to $\pm 0.180°$.

Payload optical sensitivity results and design updates were summarized. Nominal machine tolerances are 127 μm (0.005") for non-critical dimensions and 25.4 μm (0.001") for critical dimensions. A Zemax model of the optical train for was used for tolerancing sensitivity analysis. This led to the addition of a kinematic adjustment in piston for L2, the elimination of the quadcell focusing lens, and the addition of a shim adjustment in piston for the telescope to adjust the quadcell spot size.

Finally, the thermal model development for the CLICK B/C payload was described. The electronics used are industrial grade where possible, with an extended operational temperature range from -40°C to 85°C. The limiting components were the EDFA, with an operational temperature range of 0°C to 65°C, and the camera, with an operational temperature range of -40°C to 45°C. The interface between the payload and the spacecraft was defined between -10°C and 25°C. The payload modes define different heat loads for the power drawing components. The thermal design maintains a 10°C margin from the survival temperature ratings of all components.

Future work includes a comprehensive survey of pointing loss versus range for the open-loop spacecraft coarse stage tracking crosslink PAT mode (CSTOL); analysis of the value of scanning manuevers during spacecraft CSTOL for reducing pointing error performance requirements; a comprehensive survey of downlink performance variations and operational distinctions in LEO orbits; a more detailed finite element analysis for thermoelastic deformations of the payload optical bench using the thermal model described; assembly, optical calibration, and environmental testing of the payload EDU.

The CLICK B/C technology demonstration will enable mission concepts including space radio interferometry, GPS-denied navigation, time synchronization for synthetic aperture telescopes, and improved bandwidth for science data telemetry on size, weight, and power limited platforms like nanosatellites.

Acknowledgments

The mission is a collaboration between the MIT Space, Telecommunications, Astronomy, and Radiation (STAR) Lab, University of Florida's Precision Space Systems Lab (PSSL), and NASA Ames Research Center (ARC). This work was funded by the CLICK (CubeSat Laser Infrared CrosslinK) Technology Demonstration Mission, Grant Number 80NSSC18K1579. The views, opinions, and/or findings contained in this work are those of the authors and should not be interpreted as representing the official views or policies, either expressed or implied, of the National Aeronautics and Space Administration.

References

[1] Ondrej Čierny, Paul Serra, William Kammerer, Peter Grenfell, Grant Gunnison, Joseph Kusters, Cadence Payne, Paula do Vale Pereira, Kerri Cahoy, Tyler Ritz, John Conklin, David Mayer, Jan Stupl, and John Hanson. Testing of the CubeSat Laser Infrared CrosslinK (CLICK-A) Payload. In *Proceedings of the 34th AIAA/USU Conference on Small Satellites*, 2020.

[2] Peter Grenfell. GNSS-Based Relative Navigation for LEO Nanosatellite Laser Communications. Master's Thesis. Massachusetts Institute of Technology. 2020.

[3] William L. Casey and Stephen G. Lambert. *Laser Communications in Space*. Artech House Inc, Norwood, 1995.

[4] Emily B Clements. *Probabilistic Methods for Systems Engineering with Application to Nanosatellite Laser Communications*. PhD thesis, Massachusetts Institute of Technology, 2018.

[5] Emily Clements, Derek Barnes, Ryan Kingsbury, and Caleb Ziegler. Nanosatellite optical downlink experiment : design , simulation , and prototyping. 2018.

[6] Ryan Kingsbury. *Optical Communications for Small Satellites*. PhD thesis, Massachusetts Institute of Technology, 2015.

[7] Laura Yenchesky, Ondrej Cierny, Peter Grenfell, William Kammerer, Paula Do, Vale Periera, Tao Sevigny, and Kerri Cahoy. Optomechanical Design and Analysis for

Nanosatellite Laser Communications. In *Proceedings of the 33rd AIAA/USU Conference on Small Satellites*, 2019.

[8] James Paul Mason, Matt Baumgart, Bryan Rogler, Chloe Downs, Margaret Williams, Thomas N. Woods, Scott Palo, Phillip C. Chamberlin, Stanley Solomon, Andrew Jones, Xinlin Li, Rick Kohnert, and Amir Caspi. MinXSS-1 CubeSat On-Orbit Pointing and Power Performance: The First Flight of the Blue Canyon Technologies XACT 3-axis Attitude Determination and Control System. 2017.

[9] Joel Shields, Christopher Pong, Kevin Lo, Laura Jones, Swati Mohan, Chava Marom, Ian Mckinley, William Wilson, and Luis Andrade. Characterization of CubeSat Reaction Wheel Assemblies. *Journal of Small Satellites*, 6(1):565–580, 2017.

[10] Kathleen Riesing. Portable Optical Ground Stations for Satellite Communication. PhD Thesis. Massachusetts Institute of Technology. 2018.

[11] Kathleen Riesing, Hyosang Yoon, and Kerri Cahoy. A portable optical ground station for low-earth orbit satellite communications. *2017 IEEE International Conference on Space Optical Systems and Applications*, 2017.

[12] H T Yura. Threshold detection in the presence of atmospheric turbulence. *Applied Optics*, 34(6):1097–1102, 1995.

[13] Michael J Long. Pointing Acquisition and Tracking Design and Analysis for CubeSat Laser Communication Crosslinks. Master's Thesis. Massachusetts Institute of Technology. 2018.

[14] Web Page. Optical black - keeping your black anodized components black, while improving absorbance and reducing reflectivity in optical pathways by 85%. https://www.pioneermetal.com/blog/optical-black-featured-finish-anodizing-process/. 2019.